applied sciences

MDPI

Article

The Role of the Directivity of Various THz Detectors in Multiplexing Systems

Paweł Komorowski [1,*], Agnieszka Siemion [2], Michał Walczakowski [1] and Przemysław Zagrajek [1]

[1] Institute of Optoelectronics, Military University of Technology, Gen. S. Kaliskiego 2, 00908 Warsaw, Poland; michal.walczakowski@wat.edu.pl (M.W.); przemyslaw.zagrajek@wat.edu.pl (P.Z.)
[2] Faculty of Physics, Warsaw University of Technology, Koszykowa 75, 00662 Warsaw, Poland; agnieszka.siemion@pw.edu.pl
* Correspondence: pawel.komorowski@wat.edu.pl

Featured Application: Multi-focal-spot lenses as well as the knowledge of the applicability of various detectors to setups including such optics can be crucial in the development of future multiplexing systems for wireless multichannel THz transmission. The results presented could be applied to any device benefiting from a wider bandwidth of the THz data transmission channel (e.g., in telecommunication or tomography).

Abstract: Many modern and future systems, based on the wireless communication at the THz frequencies, could benefit from multichannel transmission. One of the possible approaches is to (de)multiplex several separate signals to and from a single transmission channel using dedicated diffractive optical elements. Proper selection of receivers for such systems is crucial and strongly depends not only on the frequencies used but also on the geometry of the setup. In this article, we present a complex analysis of the applicability of various detectors for the characterization of highly convergent and off-axis beams. Three three-focal-spot diffractive lenses have been designed, optimized and manufactured to verify the influence of parameters such as focal length, focal position shift, deflection angle or radiation frequency on the proper detection and separation of focal spots using different receivers. The reliable characterization of multi-focal-point structures can be performed only with high-acceptance-angle detectors, such as, for example, field-effect transistors equipped with a patch antenna. On the other hand, for the detection of a single demultiplexed signal, a much more directive receiver can be applied, as long as it is placed at a proper angle.

Keywords: THz; telecommunication; multiplexing; THz detectors; diffractive optical elements; 3D printing; MIMO systems

Citation: Komorowski, P.; Siemion, A.; Walczakowski, M.; Zagrajek, P. The Role of the Directivity of Various THz Detectors in Multiplexing Systems. *Appl. Sci.* **2022**, *12*, 3545. https://doi.org/10.3390/app12073545

Academic Editor: Dimitrios Zografopoulos

Received: 22 February 2022
Accepted: 28 March 2022
Published: 31 March 2022

1. Introduction

In recent decades, terahertz (THz) radiation and its applications have attracted the interest of a constantly increasing number of scientists and entrepreneurs [1]. The ever-growing global demand for innovation has already found many applications for THz technologies in areas such as medicine [2,3], non-destructive testing [4,5], detection of dangerous materials and objects [6,7], or telecommunication [8–11]. Despite a consistent progress in the methods of generation, detection and manipulation of the THz waves, the need for the improvement of existing technologies and the development of new ones is as strong as ever. One of the interesting possibilities is the use of diffractive optical elements (DOEs) for the formation of almost arbitrarily chosen amplitude and phase patterns [12]. This is especially appealing in the lower-frequency part of the THz spectrum, because of the wavelength dependence of diffractive patterns. The size of the smallest details of DOEs depends on the design wavelength (DWL) and it is usually in the order of small fractions of it. An analogy to the visible spectrum may be useful, where optical elements

with a roughness not exceeding $\lambda/4$ are considered sufficiently good, for example, in holography [13]. Therefore, with the DWL in the order of single millimeters or its fractions, DOEs can be fabricated with a relatively simple and very cost-efficient technique of additive manufacturing, whereas structures designed for visible or near-infrared light require much more advanced manufacturing methods, such as photolithography, laser ablation [14,15] or electron-beam lithography [16].

One of the unique solutions achievable with diffractive optics is multi-focal-point lenses with a large f-number value (the ratio of focal length to the diameter of the structure). Such elements allow radiation to be focused on several precisely defined spots in a single focal plane, which could be used in dedicated systems for multiplexing of the wireless THz data transmission channel, tomography or imaging. The concept of three-focal-spot diffractive THz lenses, as well as the iterative optimization algorithm, have already been described in our previous papers [17,18]. These results have shown that a reliable characterization of such elements can be a challenge on its own. The precise knowledge of the effects introduced by the detector parameters (such as, for example, directivity) on the distribution of registered focal points is even more important from the perspective of the application of such structures to multiplexing systems. In this article, we focus on the issue of the applicability of various detectors to multiplexing setups based on multi-focal-point lenses. It has been realized not only by the characterization of the detectors but also by experimental verification of three-focal-point lenses with high f numbers, analyzing and comparing different types of THz receivers, focal point distributions and detector configurations.

2. Materials and Methods

2.1. Detectors

Four different detectors have been used in the experimental evaluation. Three of them are based on Schottky diodes, and the fourth is based on a field-effect transistor (FET). The first three are zero-biased detectors, while FET needs a gate voltage—in our case, 1V was applied. The Schottky diode detectors were obtained commercially from Virginia Diodes, Inc. Photographs of the detectors used can be seen in Figure 1.

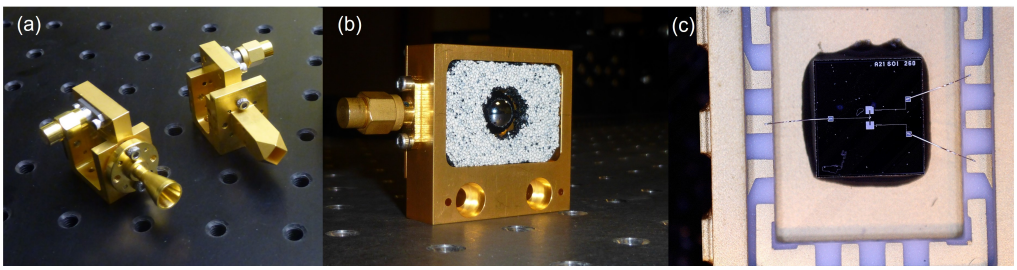

Figure 1. Photographs of the detectors used in the experiments: (**a**) Schottky diodes in the waveguides with horn antennas (two different waveguides inside); (**b**) Schottky diode with hemispherical lens and (**c**) field-effect transistor with patch antenna.

Two detectors (WR51 and WR34) were mounted inside the WR-5.1 and WR-3.4 waveguides, limiting the frequency band to the ranges of 140–220 GHz and 220–330 GHz, respectively. Detectors employ a simple conical horn (WR51) and a diagonal horn (WR34) to couple the power from the free space. According to the manufacturer, the gains of these antennas are equal to 21 dB (for WR51) and 26 dB (for WR34).

In the third detector (QOD—Quasi-Optical Detector), the Schottky diode was attached to a log-periodic planar antenna and mounted on the flat surface of an HR-Si (High-Resistivity Silicon) hemispherical lens. This antenna and lens configuration has a directivity of about 24–30 dB [19]. This quasi-optical detector works in a wide range of frequencies from 0.1 to 1 THz.

The last detector (FET) was a silicon MOSFET manufactured by the Institute of Electron Technology in Warsaw in cooperation with the Institute of Radioelectronics and Multimedia

Technology of the Warsaw University of Technology. The transistor was fabricated on a 40 µm membrane etched within the SOI (Silicon On Insulator) substrate [20]. The source and gate electrodes were connected via microstrip transmission lines to a patch antenna [21]. The antenna was designed for a 250–270 GHz band. The typical directivity for patch antennas is approximately 5–7 dB [22]. All three transistor electrodes were connected through bonded gold wires (aprox. 2 mm long) to external leads in a ceramic holder.

The antenna directivity parameter allows us to roughly predict which detector should be better suited for the characterization of highly convergent beams. However, it does not provide quantitative information on the geometric limitations of optical systems in which these detectors may be used. Therefore, in this paper, we focus on directivity, expressed as an acceptance angle.

2.2. Three-Focal-Spot Lenses

Three three-focal-spot diffractive THz lenses were designed, optimized, simulated and manufactured. The first structure realizes the symmetric distribution of focal spots with respect to the optical axis of the system and is characterized by the focal length $f = 700$ mm and the design wavelength (DWL) corresponding to the frequency of 140 GHz. The second and third structures were designed to focus the radiation into three focal spots in the asymmetric configuration (one central spot and two shifted to the same side of the optical axis) at a distance of $f = 100$ mm from the structure. The DWLs of these two structures correspond to the frequencies of 140 GHz and 260 GHz, respectively. For all DOEs, the focal spots are positioned 25 mm from each other. This means that in the case of symmetric structure, the focal spot positions with respect to the optical axis are equal to (−25) mm, 0 mm and 25 mm. On the other hand, for the asymmetric structure, the focal spots are placed at 0 mm, 25 mm and 50 mm. For readability, the focal spots placed at (−25) mm, 0 mm, 25 mm and 50 mm will be referred to as R (right), M (middle), L (left) and 2L (far left), respectively.

The geometric parameters (diameters and focal lengths) of the lenses were chosen to reflect the 3 dB acceptance cones of the highest and least directive detectors. This can be seen in Figure 2.

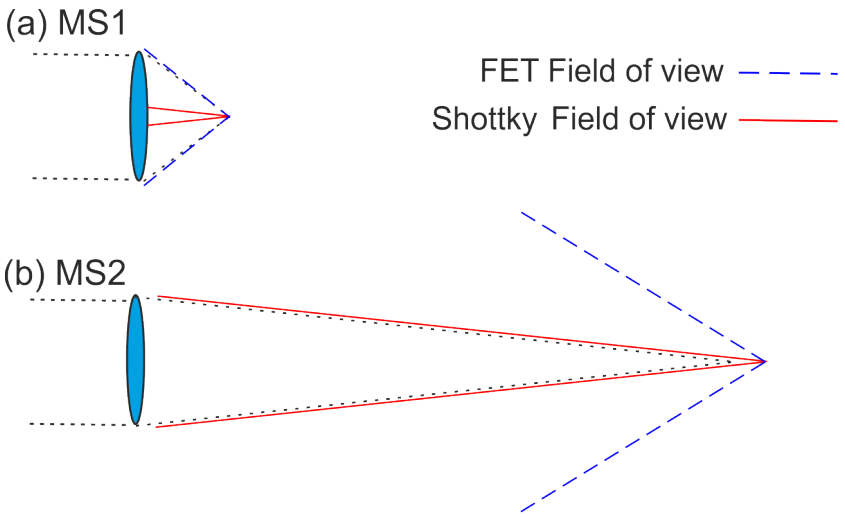

Figure 2. Simplified diagram presenting the detector field of view in relation to measured structures (MS)—(**a**) MS1—DOE with $f = 100$ mm and (**b**) MS2—DOE with $f = 700$ mm.

The configuration presented in Figure 2b shows that in the setups with a sufficiently high ratio of the focal length to the diameter of the beam (or structure), even highly directive detectors could be applied. Such multiplexing systems, however, would be either very bulky (due to length) or suffer from low channel separability (due to the narrow beam). Therefore, geometries similar to the one presented in Figure 2a have to be considered.

All structures were fabricated using the additive manufacturing method. The photographs of the manufactured DOEs are shown in Figure 3.

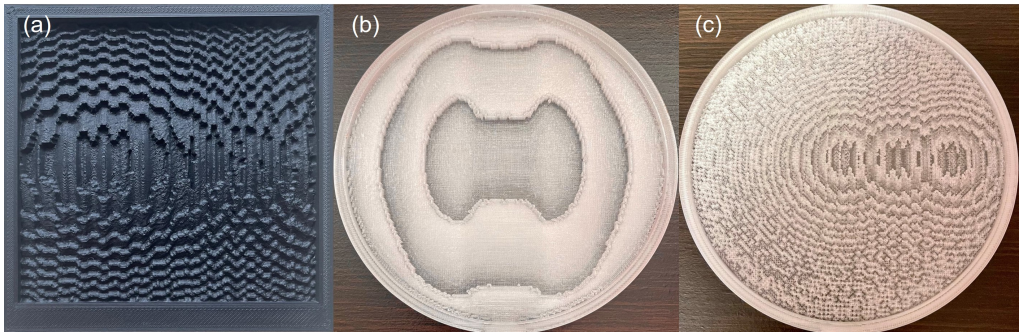

Figure 3. Photographs of the manufactured three-focal-spot lenses: (**a**) $f = 100$ mm, $\nu = 140$ GHz; (**b**) $f = 700$ mm, $\nu = 140$ GHz and (**c**) $f = 100$ mm, $\nu = 260$ GHz.

All structures were manufactured using a simple and cost-effective extrusion-based 3D printing technique. For the first DOE, polypropylene (PP Black Fiberlogy) was used, while the other two structures were fabricated from cyclic olefin copolymer (COC [TOPAS] Creamelt). The absorption coefficients of these two materials are equal to 0.21 cm^{-1}, 0.05 cm^{-1} and 0.08 cm^{-1} for PP @ 140 GHz, COC @ 140 GHZ and COC @ 260 GHz, respectively. Therefore, the average absorption losses introduced by these three structures are equal to 4.7%, 1.3% and 1.3%. The refractive indices of these materials in the sub-THz spectrum are close to 1.5, which translates to Fresnel losses below 5%. Additionally, in the design of the third structure ($f = 100$ mm, $\nu = 260$ GHz) a new 3D-modeling method, based on the extraction of blocks instead of triangle interpolation, was applied. This method allows for a more accurate representation of the numerically simulated bitmap in the 3D space. Such an approach is crucial for structures with high variance of the height of adjacent pixels (such as the one in Figure 3c) and has been described more closely in [23]. This article focuses mostly on the methodology of the characterization of off-axis beams with detectors of varying types and parameters and their applicability to multiplexing systems. The selection of diffractive structures used for this comparison reflects the evolution of the design and manufacturing methods we developed. Three-focal-spot structures have already been described in [18]. However, some new conclusions in this regard shall also be formulated.

2.3. Experimental Setup

The experiment was conducted in a straightforward optical setup, shown in Figure 4. A tunable frequency multiplier from Virginia Diodes, Inc. was used as a source of radiation. To form the divergent beam from the source into a collimated shape with a quasi-Gaussian distribution, the beam was directed to an 8″ parabolic mirror placed in such a way that the source was at its focal point $f_m = 600$ mm. The reflected beam with the desired geometry was used to illuminate the measured structure (MS) positioned around 700 mm from the mirror. To ensure independence from the lens shape, in all cases, a circular aperture was placed in front of the structure.

The detection plane is perpendicular to the main optical axis of the system. Its distance from the measured structure can be set according to the focal length of the lens. In our experiments, it was equal to 100 mm (F1) or 700 mm (F2). The detectors were mounted on motorized stages, which allows precise control of their position in the three perpendicular axes, as well as rotation along the vertical axis (θ).

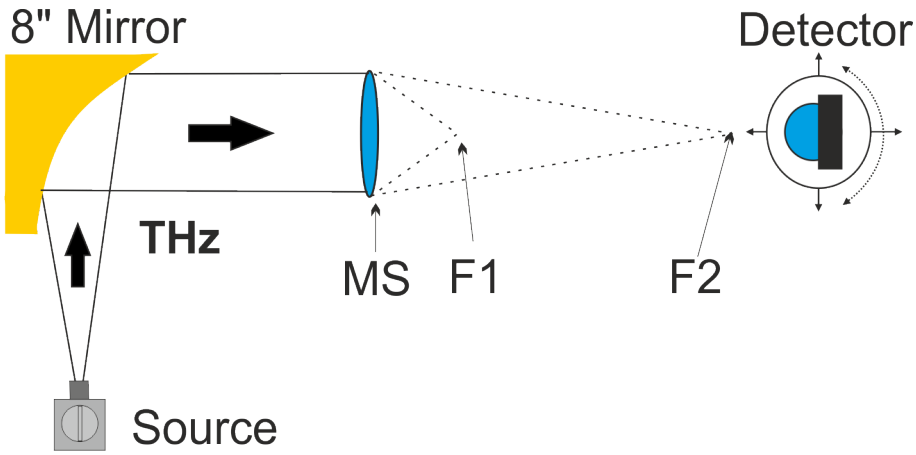

Figure 4. Simplified schematic diagram of the experimental setup. (MS)—Measured Structure, (F1)—100 mm focal point, (F2)—700 mm focal point.

3. Results

3.1. Characterisation of the Detectors

First, all four investigated detectors were characterized for the acceptance angle of the incoming radiation. The comparison of the angular dependencies observed for the FET, QOD, WR34 and WR51 detectors can be seen in Figure 5.

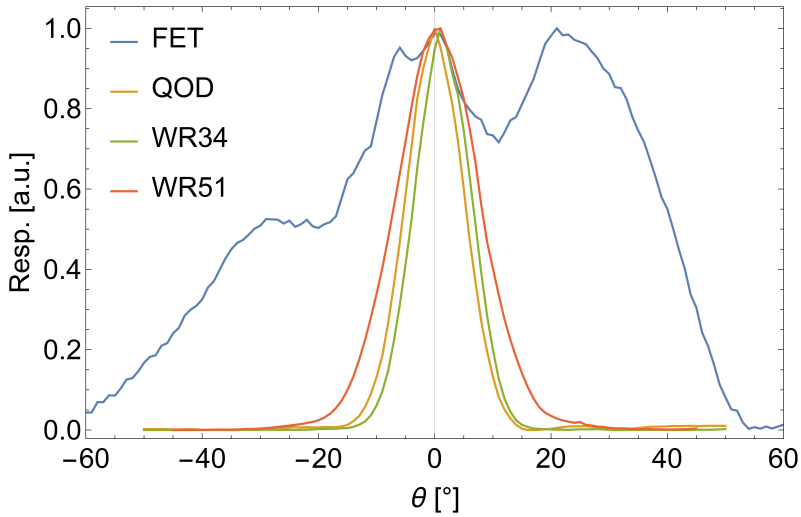

Figure 5. The comparison of the normalized angular acceptance characteristics obtained for the FET (at 260 GHz), QOD (at 140 GHz), WR34 (at 260 GHz) and WR51 (at 140 GHz) detectors, marked with the blue, orange, green and red lines, respectively.

As can be seen, the widest acceptance band is observed for the FET detector. The other three are much more sensitive to the angle of incident radiation. The calculated 3 dB bandwidth (the average angle at which the registered signal decreased twice) for the FET, QOD, WR34 and WR51 detectors is equal to 69°, 12°, 11° and 16°, respectively.

In the next step, the frequency dependence of the angular acceptance was also tested for all investigated detectors. The results are presented in Figure 6.

For the QOD, WR34 and WR51 detectors, changes in the angular acceptance band can be noticed only for relatively large shifts in the frequency (in the order of tens of GHz). The general tendency for all of these detectors is that the higher the frequency of radiation, the narrower the angular acceptance band. The situation is different for the FET detector, where small shifts in the radiation frequency (in the order of a single GHz) result in significant distortions of the angular acceptance characteristic. Most probably it is the combined effect of the patch antenna the detector is equipped with, and three wires connected to

the transistor terminals (visible in Figure 1c). These wires have lengths in the order of the wavelength of the incoming radiation and thus may form an unintentional antenna with unspecified characteristics and strong frequency dependence. The possible influence of the shape and direction of the beam has been experimentally eliminated by upside down inversion of the FET detector (Figure 7).

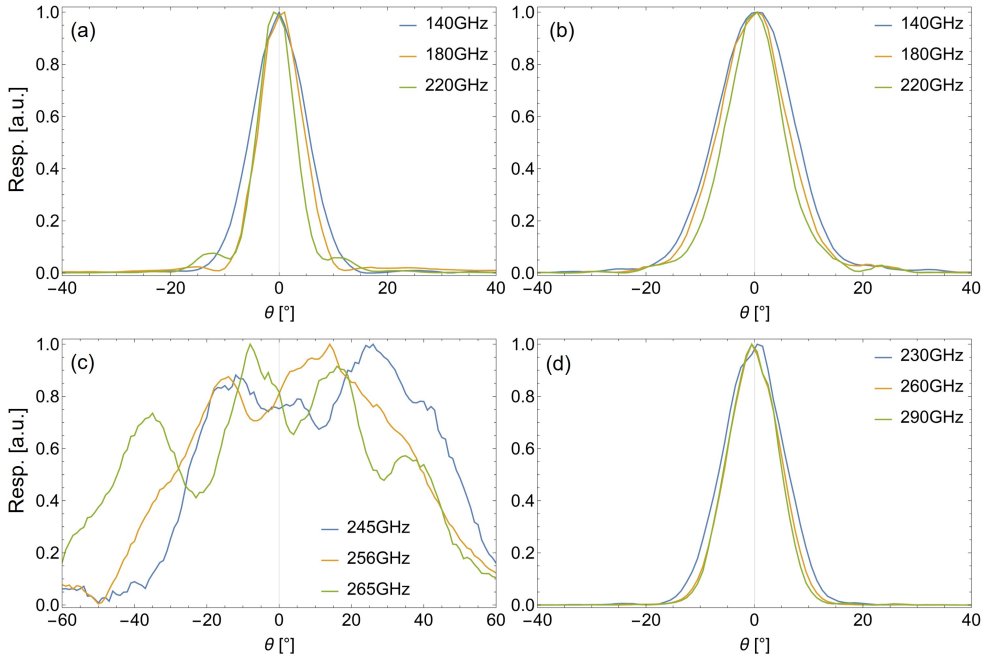

Figure 6. Frequency dependence of the angular characteristics of the detectors: (**a**) QOD, (**b**) WR51, (**c**) FET and (**d**) WR34.

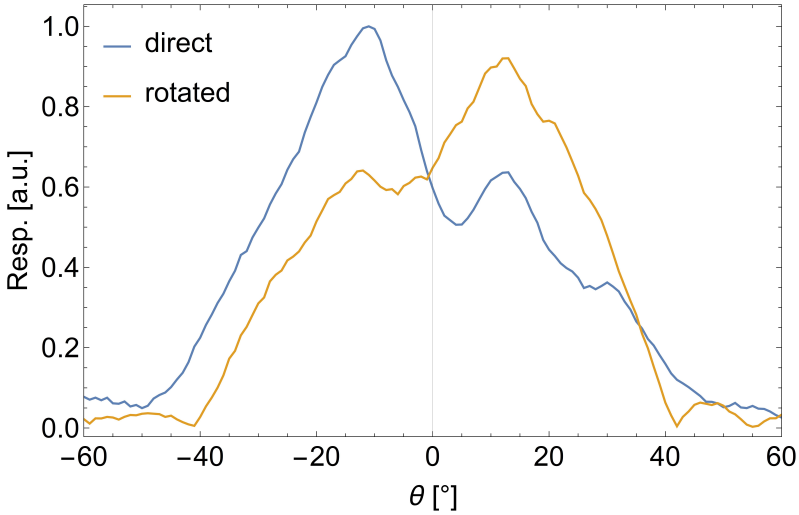

Figure 7. Comparison of the angular acceptance characteristics of the detector in nominal position (blue line) and rotated by 180° (orange line).

As can be seen in Figure 7, the angular acceptance characteristic obtained with the rotated detector is axially symmetric to the nominal one with respect to the $\theta = 0°$ line.

3.2. Examination of the Three-Focal-Spot Lenses

Three designed three-focal-spot THz lenses were experimentally verified using the detectors corresponding to the DWL. In all cases, the focal spots were observed at the desired positions. However, verifying the relative intensity of these focal spots is not trivial.

Most clearly, it can be seen by comparison of the measurements performed for structures with different focal lengths. One-dimensional cross sections along the three spots in the focal plane formed by the structure with focal length $f = 700$ mm are presented in Figure 8.

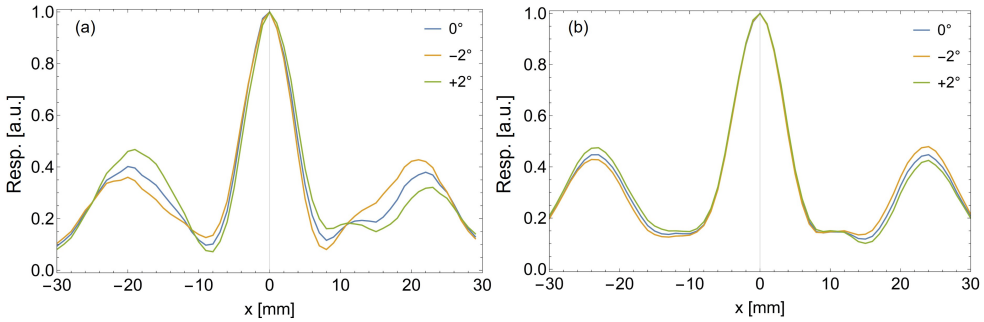

Figure 8. Cross sections along the spots measured in the focal plane of the $f = 700$ mm structure with (**a**) QOD and (**b**) WR51 detectors. The blue, orange and green lines denote the configurations with the detectors placed at an angle of $0°$, $+2°$ and $-2°$, respectively. These geometries reflect the situations in which the detectors face the center of the lens from the positions of M, L and R focal spots.

For a focal length equal to 700 mm and a focal spot shift equal to 25 mm, the radiation deflection angle is approximately $2°$. However, even for such a small angle, the differences in the readings are clearly visible. When the detector faces the center of the lens from the position of one of the side focal spots (L or R), the observed relative intensity of this focal spot increases. It can also be seen that the effect is stronger for the detector with the narrower angular acceptance band—QOD (Figure 8a).

Nevertheless, in such a configuration with a high ratio of the focal length to the focal point shift, the structure can be reliably verified even with strongly directive detectors. It also means that the directivity of the utilized detector would not be crucial in multiplexing systems using such multi-focal-spot lenses. The issue lies, however, in the need for the minimization of the devices. The high focal length to focal point shift ratio can be achieved either by long focal length or by small focal point shift. The first option results in a large device with a length close to a meter, while the second option does not allow the simultaneous detection of different signals with bulky detectors. Hence, the only solution is to reduce the ratio of the focal length and the focal point shift, which results in a higher deflection angle of the incoming radiation. To illustrate this issue, let us evaluate the three-focal-spot structure with a focal length $f = 100$ mm. The cross sections of the spots in the focal plane measured with the QOD and WR51 detectors placed at different angles are shown in Figure 9.

In this case, the deflection angles of the radiation forming the L and 2L focal spots are equal to ca. $14°$ and $27°$, respectively. Therefore, the results differ much more strongly between detector types as well as the detector positions. All three lines in Figure 9a,b are in scale with each other. For the sake of clarity of comparison, all results have been normalized for the highest signal observed for a given detector. One can easily notice that in both cases the intensity of the middle focal spot is the highest for the detector facing it (perpendicular to the optical axis, marked as rotated by $0°$). This is an expected result for highly directive detectors. However, the results are less intuitive for the shifted focal spots. The intensity of the L focal spot is the highest in the direct detector configuration instead of the theoretically favored tilted by $14°$ configuration. On the other hand, the highest intensity of the 2L focal spot has been observed exactly in the tilted by $14°$ configuration instead of the theoretically favored—in this case—tilted by $27°$ configuration. The differences between the relative intensities of the focal spots observed for different detection angles are also greater for the detector with a narrower angular acceptance band (QOD).

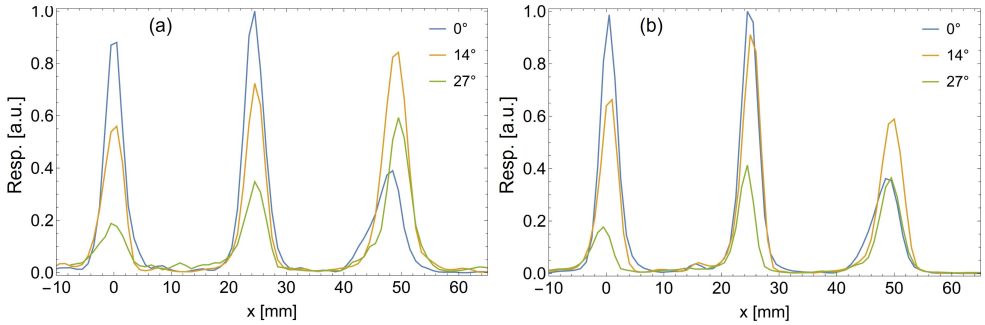

Figure 9. Cross sections along the spots measured in the focal plane of the $f = 100$ mm and $\nu = 150$ GHz structure with (**a**) QOD and (**b**) WR51 detectors. Blue, orange and green lines denote the configurations with the detectors placed at an angle of 0°, 14° and 27°, respectively. These geometries reflect the situations in which the detectors face the center of the lens from the positions of M, L and 2L focal spots.

An analogous structure has also been manufactured for the DWL corresponding to the frequency of 260 GHz. This frequency has been dictated by the bandwidth of this particular FET detector used in our laboratory. The results can be seen in Figure 10.

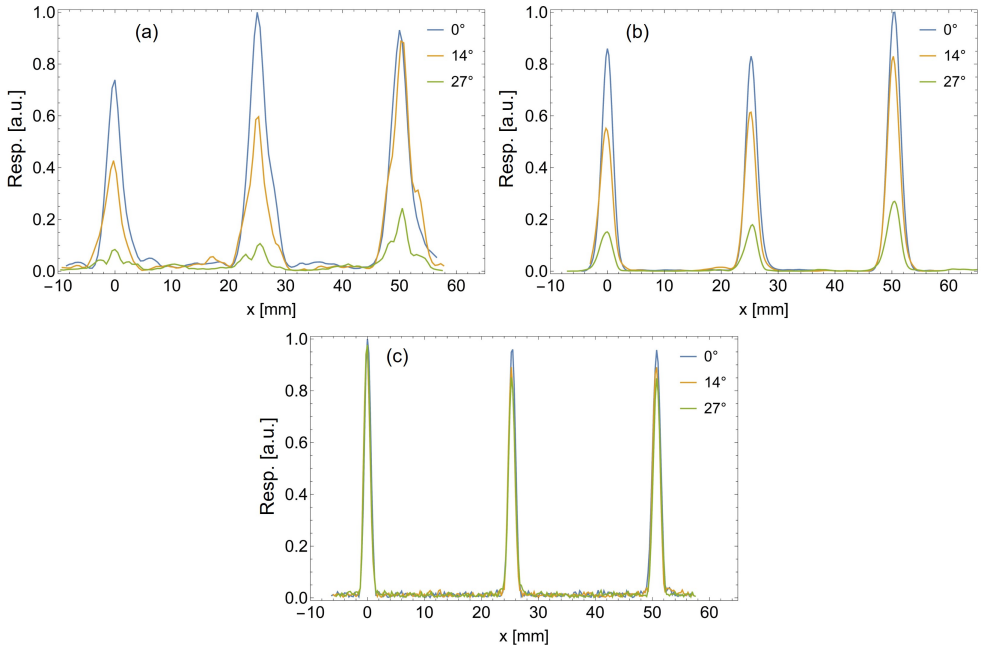

Figure 10. Cross sections along the spots measured in the focal plane of the $f = 100$ mm and $\nu = 260$ GHz structure with (**a**) QOD, (**b**) WR34 and (**c**) FET detectors. The blue, orange and green lines denote the configurations with the detectors placed at an angle of 0°, 14° and 27°, respectively. These geometries reflect the situations in which the detectors face the center of the lens from the positions of M, L and 2L focal spots.

As can be seen, the intensity distributions obtained with the QOD and WR34 detectors placed at different angles also differ strongly in this case. At this frequency, however, the highest intensity in all focal spots has been observed for the direct detector configuration. On the other hand, the relative intensity of the focal spots changes for different detector angles, which shows that the reliable determination of the actual or relative intensities is extremely hard, if not infeasible. The intensity distributions obtained with the FET detector (Figure 10c) are, however, much more reliable. Firstly, it must be noted that the relative intensities of the M, L and 2L focal spots are almost equal (1.00, 0.97 and 0.96, respectively). Secondly, the influence of the detector rotation, in comparison to the other two detectors,

is far less significant. The relative intensities of the L and 2L focal spots compared to the intensity of the M spot dropped to 0.93, 0.93 and 0.87, 0.87 when observed with the detector rotated by 14° and 27°, respectively. Moreover, it should be noted that the intensities of the shifted focal spots (L and 2L) are reduced in the theoretically favored configurations with the FET detector facing the center of the lens.

4. Discussion

First, it should be underlined that all designed three-focal-spot diffractive lenses have been positively verified experimentally. The structures focus the THz radiation of a given frequency onto three separate focal spots lying in the same focal plane. The first two structures ($f = 700$ mm, $\nu = 140$ GHz in Figure 8 and $f = 100$ mm, $\nu = 140$ GHz in Figure 9) generate focal spots of unequal intensity. As already explained in [23], it is most likely related to the 3D model rendering method. In this case, pixels of the 2D bitmap obtained in the simulations have been extended and interpolated to form a popular triangle mesh. The last DOE ($f = 100$ mm, $\nu = 260$ GHz in Figure 10) was manufactured with the new method, rendering the 3D model as a set of cuboids, which complies more closely with the simulated bitmap. The experimental results have shown that this method allows us to obtain three well-defined focal spots of almost equal intensities. The issue lies, however, in the experimental validation of the structures and the characterization of the focal spot distribution. Commonly used THz detectors, equipped with the horn antenna or a silicon hemisphere, have a rather narrow angular acceptance band of the incoming radiation (16° and 12°, respectively). Thus, obtaining reliable results would require the whole DOE to be placed within the acceptance cone of the particular detector. This in turn means that the ratio of the diameter of the structure and/or the shift of the focal spots to the focal length should be sufficiently small. In fact, this happens for the $f = 700$ mm structure, where the redirection angles are as low as 2°. The experiment has shown that, in this case (Figure 8), the influence of the illumination angle is relatively insignificant. A setup that is over 70 cm long, although very convenient during laboratory experiments, most probably shall be too bulky for practical applications. Therefore, we also designed DOEs with a focal length $f = 100$ mm for much more compact setups. In these projects, the proper separation of the focal spots could have been realized only at the cost of much higher redirection angles. Moreover, from the distance of 100 mm only part of the structure lies within the acceptance cone of the bulky detectors (WR34, WR51 and QOD). This means that moving the detector changes not only the average illumination angle, but also the area of the DOE observed by the detector. The influence of these two effects on the detected focal spots can clearly be seen in Figures 9a,b and 10a,b. Not only do the relative intensities of the focal spots change for different detector positions, but also the maximal intensity value of a particular focal spot is not always registered for the theoretically favored configuration with the detector aiming at the center of the lens from the focal spot position. Therefore, the reliable characterization of the THz diffractive optics with a high f-number can only be performed with a detector much less sensitive to the direction of the incoming radiation, such as, for example, a field effect transistor with a planar antenna. An experiment has shown that such a detector allows for a much more certain verification of the three-focal-spot structure (Figure 10). The detector used is characterized by a 3 dB angular acceptance band of 69° and registered an almost uniform focal spot distribution with the maximum intensity deviation between detector configurations equal to 11%.

5. Conclusions

Foremost, the results of this research are important from the perspective of the characterization methods of the THz optics and especially THz optics with small f-number values. Utilizing bulky antennas is likely to lead to distorted measurements. Moreover, the experiments have proven that 3D printed DOEs designed using the iterative algorithm and convolution method of light propagation can efficiently redirect THz radiation into three separate focal spots. The modified block-based extrusion method of 3D-modeling

has allowed for significant improvement of the uniformity of the intensity distributions between focal spots. It clearly demonstrates that in the case of more complex diffractive elements with a high variety of pixel height, the application of dedicated methods for the modeling of 3D-shapes from simulated bitmaps becomes necessary. Such structures can be used in future THz telecommunication systems as a way to multiplex signals. It should also be noted that any kind of setup, benefiting from the increment of the information capacity of the communication channel, could be seen as a potential point of application of multi-focal-point lenses.

The results presented also point out the issue of detector directivity in systems with high deflection angles and a low focal length to diameter ratio. Although proper verification of the beam shapes can only be realized with high-angular-bandwidth receivers, the application of more directive ones is also possible. In such a case, individual adjustment of the detector's placement (including the angle of rotation) is necessary.

Author Contributions: Conceptualization, P.K., A.S. and P.Z.; methodology, P.K., M.W. and P.Z.; software, P.K. and P.Z.; validation, P.K., A.S., M.W. and P.Z.; formal analysis, P.K.; investigation, P.K. and M.W.; resources, M.W. and P.Z.; data curation, P.K. and M.W.; writing—original draft preparation, P.K.; writing—review and editing, A.S., M.W. and P.Z.; visualization, P.K. and M.W.; supervision, A.S. and P.Z.; project administration, A.S. and P.Z.; funding acquisition, A.S. and P.Z. All authors have read and agreed to the published version of the manuscript.

Funding: The research was funded by the National Science Centre, Poland under the OPUS-18 programme (2019/35/B/ST7/03909).

Data Availability Statement: The data presented in this study are available upon request from the corresponding author. The data are not publicly available due to the qualitative nature and all transcribed data are being kept in a different form.

Acknowledgments: The authors would like to thank Patrycja Czerwińska and Mateusz Kałuża from Faculty of Physics, Warsaw University of Technology for the help in the process of designing and manufacturing of the diffractive structures.

Conflicts of Interest: The authors declare no conflict of interest. The funders had no role in the design of the study; in the collection, analyses, or interpretation of data; in the writing of the manuscript, or in the decision to publish the results.

Abbreviations

The following abbreviations are used in this manuscript:

DOE	Diffractive Optical Element
DWL	Design Wavelength
FET	Field-effect transistor
QOD	Quasi-Optical Detector

References

1. Irizawa, A.; Lupi, S.; Marcelli, A. Terahertz as a Frontier Area for Science and Technology. *Condens. Matter* **2021**, *6*, 23. [CrossRef]
2. Pickwell, E.; Wallace, V. Biomedical applications of terahertz technology. *J. Phys. D Appl. Phys.* **2006**, *39*, R301. [CrossRef]
3. Zhang, Y.; Wang, C.; Huai, B.; Wang, S.; Zhang, Y.; Wang, D.; Rong, L.; Zheng, Y. Continuous-Wave THz Imaging for Biomedical Samples. *Appl. Sci.* **2021**, *11*, 71. [CrossRef]
4. Tao, Y.H.; Fitzgerald, A.J.; Wallace, V.P. Non-contact, non-destructive testing in various industrial sectors with terahertz technology. *Sensors* **2020**, *20*, 712. [CrossRef] [PubMed]
5. Hlosta, P.; Nita, M.; Powala, D.; Świderski, W. Terahertz radiation in non-destructive testing of composite pyrotechnic materials. *Compos. Struct.* **2022**, *279*, 114770. [CrossRef]
6. Leahy-Hoppa, M.R.; Fitch, M.J.; Osiander, R. Terahertz spectroscopy techniques for explosives detection. *Anal. Bioanal. Chem.* **2009**, *395*, 247–257. [CrossRef] [PubMed]
7. Tzydynzhapov, G.; Gusikhin, P.; Muravev, V.; Dremin, A.; Nefyodov, Y.; Kukushkin, I. New real-time sub-terahertz security body scanner. *J. Infrared Millim. Terahertz Waves* **2020**, *41*, 632–641. [CrossRef]
8. Saeed, A.; Gurbuz, O.; Akkas, M.A. Terahertz communications at various atmospheric altitudes. *Phys. Commun.* **2020**, *41*, 101113. [CrossRef]

9. Horst, Y.; Blatter, T.; Kulmer, L.; Bitachon, B.I.; Baeuerle, B.; Destraz, M.; Heni, W.; Koepfli, S.; Habegger, P.; Eppenberger, M.; et al. Transparent optical-THz-optical Link transmission over 5/115 m at 240/190 Gbit/s enabled by plasmonics. In Proceedings of the 2021 Optical Fiber Communications Conference and Exhibition (OFC), San Francisco, CA, USA, 6–10 June 2021; pp. 1–3.
10. Moon, S.R.; Sung, M.; Lee, J.K.; Cho, S.H. Cost-effective photonics-based THz wireless transmission using PAM-N signals in the 0.3 THz band. *J. Light. Technol.* **2021**, *39*, 357–362. [CrossRef]
11. Valušis, G.; Lisauskas, A.; Yuan, H.; Knap, W.; Roskos, H.G. Roadmap of terahertz imaging 2021. *Sensors* **2021**, *21*, 4092. [CrossRef] [PubMed]
12. Siemion, A. The magic of optics—An overview of recent advanced terahertz diffractive optical elements. *Sensors* **2021**, *21*, 100. [CrossRef] [PubMed]
13. Stover, J.C. *Optical Scattering. Measurement and Analysis*; SPIE Optical Engineering Press: Bellingham, WA, USA, 1995.
14. Minkevičius, L.; Voisiat, B.; Mekys, A.; Venckevičius, R.; Kašalynas, I.; Seliuta, D.; Valušis, G.; Račiukaitis, G.; Tamošiŭnas, V. Terahertz zone plates with integrated laser-ablated bandpass filters. *Electron. Lett.* **2013**, *49*, 49–50. [CrossRef]
15. Tamošiūnaitė, M.; Indrišiūnas, S.; Tamošiūnas, V.; Minkevičius, L.; Urbanowicz, A.; Račiukaitis, G.; Kašalynas, I.; Valušis, G. Focusing of terahertz radiation with laser-ablated antireflective structures. *IEEE Trans. Terahertz Sci. Technol.* **2018**, *8*, 541–548. [CrossRef]
16. O'Shea, D.C.; Suleski, T.J.; Kathman, A.D.; Prather, D.W. *Diffractive Optics: Design, Fabrication, and Test*; SPIE Press: Bellingham, WA, USA, 2004; Volume 62.
17. Siemion, A.; Komorowski, P.; Surma, M.; Ducin, I.; Sobotka, P.; Walczakowski, M.; Czerwińska, E. Terahertz diffractive structures for compact in-reflection inspection setup. *Opt. Express* **2020**, *28*, 715–723. [CrossRef] [PubMed]
18. Komorowski, P.; Czerwińska, P.; Surma, M.; Zagrajek, P.; Piramidowicz, R.; Siemion, A. Three-focal-spot terahertz diffractive optical element-iterative design and neural network approach. *Opt. Express* **2021**, *29*, 11243–11253. [CrossRef] [PubMed]
19. Hesler, J.L.; Liu, L.; Xu, H.; Duan, Y.; Weikle, R.M. The development of quasi-optical THz detectors. In Proceedings of the 2008 33rd International Conference on Infrared, Millimeter and Terahertz Waves, Pasadena, CA, USA, 15–19 September 2008; pp. 1–2.
20. Kopyt, P.; Salski, B.; Marczewski, J.; Zagrajek, P.; Lusakowski, J. Parasitic effects affecting responsivity of sub-THz radiation detector built of a MOSFET. *J. Infrared Millim. Terahertz Waves* **2015**, *36*, 1059–1075. [CrossRef]
21. Kopyt, P.; Salski, B.; Zagrajek, P.; Obrębski, D.; Marczewski, J. Modeling of silicon-based substrates of patch antennas operating in the sub-THz range. *IEEE Trans. Terahertz Sci. Technol.* **2017**, *7*, 424–432. [CrossRef]
22. Kushwaha, R.K.; Karuppanan, P.; Malviya, L. Design and analysis of novel microstrip patch antenna on photonic crystal in THz. *Phys. B Condens. Matter* **2018**, *545*, 107–112. [CrossRef]
23. Surma, M.; Kaluza, M.; Czerwińska, P.; Komorowski, P.; Siemion, A. Neural-network based approach to optimize THz computer generated holograms. *Photonics Lett. Pol.* **2021**, *13*, 88–90. [CrossRef]